# ImmunoPET/MR imaging allows specific detection of *Aspergillus fumigatus* lung infection in vivo

Anna-Maria Rolle[a,1], Mike Hasenberg[b,1], Christopher R. Thornton[c], Djamschid Solouk-Saran[b], Linda Männ[b], Juliane Weski[b], Andreas Maurer[a], Eliane Fischer[d], Philipp R. Spycher[d], Roger Schibli[d], Frederic Boschetti[e], Sabine Stegemann-Koniszewski[f,g], Dunja Bruder[f,g], Gregory W. Severin[h,i], Stella E. Autenrieth[j], Sven Krappmann[k], Genna Davies[c], Bernd J. Pichler[a], Matthias Gunzer[b,2], and Stefan Wiehr[a,2]

[a]Werner Siemens Imaging Center, Department of Preclinical Imaging and Radiopharmacy, Eberhard Karls University Tübingen, 72076 Tübingen, Germany; [b]Institute for Experimental Immunology and Imaging, University Hospital, University Duisburg-Essen, 45122 Essen, Germany; [c]Biosciences and ISCA Diagnostics Ltd., College of Life and Environmental Sciences, University of Exeter, Exeter EX4 4QD, United Kingdom; [d]Center for Radiopharmaceutical Sciences, Paul Scherrer Institute, 5232 Villigen, Switzerland; [e]CheMatech, Faculté des Sciences Mirande, 21000 Dijon, France; [f]Immune Regulation Group, Helmholtz Centre for Infection Research, 38124 Braunschweig, Germany; [g]Infection Immunology, Institute of Medical Microbiology, Infection Control and Prevention, Otto-von-Guericke University Magdeburg, 39120 Magdeburg, Germany; [h]The Hevesy Laboratory, Center for Nuclear Technologies, Technical University of Denmark, 4000 Roskilde, Denmark; [i]Center for Nanomedicine and Theranostics, Technical University of Denmark, 2800 Lyngby, Denmark; [j]Department of Hematology, Oncology, Rheumatology, Immunology and Pulmonology, University Hospital Tübingen, 72076 Tübingen, Germany; and [k]Microbiology Institute - Clinical Microbiology, Immunology and Hygiene, University Hospital Erlangen and Friedrich-Alexander University Erlangen-Nürnberg, 91054 Erlangen, Germany

Edited by Michael E. Phelps, University of California, Los Angeles, CA, and approved December 15, 2015 (received for review September 23, 2015)

**Invasive pulmonary aspergillosis (IPA) is a life-threatening lung disease caused by the fungus *Aspergillus fumigatus*, and is a leading cause of invasive fungal infection-related mortality and morbidity in patients with hematological malignancies and bone marrow transplants. We developed and tested a novel probe for noninvasive detection of *A. fumigatus* lung infection based on antibody-guided positron emission tomography and magnetic resonance (immunoPET/MR) imaging. Administration of a [$^{64}$Cu]DOTA-labeled *A. fumigatus*-specific monoclonal antibody (mAb), JF5, to neutrophil-depleted *A. fumigatus*-infected mice allowed specific localization of lung infection when combined with PET. Optical imaging with a fluorochrome-labeled version of the mAb showed colocalization with invasive hyphae. The mAb-based newly developed PET tracer [$^{64}$Cu]DOTA-JF5 distinguished IPA from bacterial lung infections and, in contrast to [$^{18}$F]FDG-PET, discriminated IPA from a general increase in metabolic activity associated with lung inflammation. To our knowledge, this is the first time that antibody-guided in vivo imaging has been used for noninvasive diagnosis of a fungal lung disease (IPA) of humans, an approach with enormous potential for diagnosis of infectious diseases and with potential for clinical translation.**

*Aspergillus fumigatus* | aspergillosis | immunoPET/MR | PET | imaging

Despite the success of therapeutics fighting against especially bacteria and fungi, infectious diseases still remain one of the main causes of death worldwide (1). Beside effective therapeutics, the early and reliable differential diagnosis of infectious diseases is of utmost importance; here noninvasive imaging can have a huge impact. Imaging of infectious diseases is an emerging field still in its infancy, but is nevertheless attracting considerable attention from many disciplines in biomedical research, as well as in patient care. There are several challenging aspects of imaging infectious diseases, not at least the clear and reliable differentiation between bacterial, fungal, and viral infection needed for the best treatment options. Furthermore, infection is typically linked to inflammation, which makes it mandatory to use pathogen specific imaging probes to definitively and rapidly diagnose the causative agent of the infectious disease.

Invasive pulmonary aspergillosis (IPA) is a frequently fatal lung disease of neutropenic patients caused by the ubiquitous airborne fungus *Aspergillus fumigatus*. As a leading cause of death in hematological malignancy and hematopoietic stem cell transplant patients, the fungus accounts for the majority of the >200,000 life-threatening infections annually with an associated mortality rate of 30–90% (2). Diagnosis of IPA is a major challenge as clinical manifestations of the disease (febrile episodes unresponsive to antibiotics, pulmonary infiltrates and radiological abnormalities) are nonspecific, and methods for the detection of circulating biomarkers such as β-D-glucan or galactomannan (GM) in the bloodstream lack specificity or sensitivity (3). For this reason, culture of the fungus from lung biopsy tissues remains the gold standard test for IPA diagnosis (4), but this invasive procedure lacks sensitivity, delays diagnosis, and is frequently not possible in neutropenic patients. Recently, detection of *A. fumigatus* GM or mannoprotein antigens in bronchoalveolar lavage (BAL) has shown enormous promise for the early detection of the disease especially when combined with point-of-care diagnostics (5). However, BAL recovery is similarly intrusive and so a sensitive, specific, and minimally invasive test that is amenable to repeated application is needed to allow diagnostic-driven treatment with antifungal drugs. Such a test should be able to discriminate between active lung infection caused by hyphal proliferation of the

## Significance

**Invasive pulmonary aspergillosis (IPA) is a frequently fatal lung disease of immunocompromised patients, and is being increasingly reported in individuals with underlying respiratory diseases. Proven diagnosis of IPA currently relies on lung biopsy and detection of diagnostic biomarkers in serum, or in bronchoalveolar lavage fluids. This study supports the use of immunoPET/MR imaging for the diagnosis of IPA, which is so far not used for diagnosis. The antibody-guided imaging technique allows accurate, noninvasive and rapid detection of fungal lung infection and discrimination of IPA from bacterial lung infections and general inflammatory responses. This work demonstrates the applicability of molecular imaging for IPA detection and its potential for aiding clinical diagnosis and management of the disease in the neutropenic host.**

Author contributions: A.-M.R., M.H., C.R.T., J.W., A.M., E.F., P.R.S., R.S., F.B., S.S.-K., D.B., G.W.S., B.J.P., M.G., and S.W. designed research; A.-M.R., M.H., C.R.T., D.S.-S., L.M., A.M., E.F., P.R.S., F.B., S.S.-K., G.W.S., S.E.A., S.K., G.D., and S.W. performed research; A.-M.R., M.H., C.R.T., A.M., P.R.S., S.E.A., G.D., and S.W. analyzed data; and A.-M.R., M.H., C.R.T., A.M., R.S., G.W.S., B.J.P., M.G., and S.W. wrote the paper.

The authors declare no conflict of interest.

This article is a PNAS Direct Submission.

Freely available online through the PNAS open access option.

[1]A.-M.R. and M.H. contributed equally to this work.

[2]To whom correspondence may be addressed. Email: stefan.wiehr@med.uni-tuebingen.de or matthias.gunzer@uni-due.de.

This article contains supporting information online at www.pnas.org/lookup/suppl/doi:10.1073/pnas.1518836113/-/DCSupplemental.



www.pnas.org/cgi/doi/10.1073/pnas.1518836113

fungus and inactive spores that are a common component of inhaled air. Conventional imaging modalities such as computed tomography (CT) and magnetic resonance imaging (MRI) are able to produce high contrast images of all structures within the human body but they are not able to distinguish between invasive fungal infections and those caused by other microorganisms, or to discriminate these from cancer tissues (6, 7). Molecular imaging using positron emission tomography (PET) is able to define the metabolic properties of living cells as well as their molecular structures when suitable radiolabeled tracers are used (8). Here, we use a radiolabeled monoclonal antibody (mAb) specific to the active growth phase of *A. fumigatus* to diagnose IPA in a neutropenic animal model of the disease with PET/MRI. Our work shows that antibody-based immunoPET can be used successfully to noninvasively identify this challenging lung disease.

## Results

We hypothesized that target-specific radiolabeled antibodies and immunoPET imaging could be used noninvasively and in vivo to detect lung infections caused by *A. fumigatus*. We used *A. fumigatus*-infected, neutrophil-depleted mice as a model of IPA to mimic the suppressed innate immunity of patients at high-risk for IPA, and chose an abundant hyphal-associated antigen as the in vivo target for immunoPET/MR imaging using the well characterized *A. fumigatus*-specific mAb JF5. The JF5 antibody binds to an extracellular mannoprotein antigen secreted during active growth of the pathogen only, and it is used in a point-of-care lateral-flow assay for detection of diagnostic antigen in human serum and BAL samples (5).

To test the immunoreactivity and the serum stability of the chelator and fluorochrome labeled mAb JF5 after modification in vitro tests were performed. Immunoreactivity of mAb JF5 following labeling with the chelator DOTA and the fluorochrome DyLight 650 was investigated by immunofluorescence using germinated spores of *A. fumigatus*. Labeling of the antibody with the chelator or the fluorochrome did not alter the hyphal-specific binding of the antibody to its target mannoprotein antigen (Fig. S1*A*). Intense fluorescence of hyphae but lack of staining of ungerminated spores of the fungus was observed in each case, consistent with binding of the antibody to the active growth phase of the pathogen. Similarly, there was no significant loss of antibody immunoreactivity in ELISA tests using a saturating concentration of purified mannoprotein antigen (Fig. S1*B*), further demonstrating that labeling of the JF5 antibody with the chelator DOTA or fluorochrome DyLight 650 had no significant effect on binding of the antibody to its target antigen. For assessment of the serum stability, one volume of [$^{64}$Cu]DOTA-JF5 in its final formulation was incubated with three volumes of C57BL/6 serum at 37 °C for various time points and immediately analyzed by Radio-HPSEC. The analysis showed no signs of proteolytic degradation, protein aggregation or copper transchelation to serum proteins over the time of 48 h under these conditions (Fig. S1 *C*–*F*).

**JF5 Antibody Binds to *A. fumigatus* in Vivo.** To test the suitability of JF5 as an intravital whole body diagnostic tool when equipped with a suitable label, we investigated first whether fluorochrome-labeled JF5 was able to detect *A. fumigatus* in infected lungs of experimental animals. Neutrophil-depleted mice were intratracheally (i.t.) infected with conidia of a genetically modified strain of the fungus expressing the fluorescent protein tdTomato (*A. fumigatus*$^{tdTomato}$; Fig. 1*A*) and, 48 h later, the lungs were excised and the presence of fungal masses was confirmed in serial sections by methenamine silver staining (Fig. 1*B*). Consecutive sections were then probed with fluorochrome-labeled JF5 or the respective fluorochrome-labeled isotype control. Here, JF5 gave an intense staining of fungal elements (Fig. 1*C*) that produced a cell-wall selective pattern, whereas isotype controls were negative (Fig. 1*C*). In a second set of experiments the labeled JF5 antibody was injected 24 h after infection into the circulation of mice (Fig. 1*D*). Lung lobes were dissected 24 h later and were analyzed by confocal microscopy. Large red fluorescent fungal masses were detected (green), which were colabeled with fluorescent JF5 (red) on individual hyphae, as well as extracellular antigen in close proximity to hyphal elements (Fig. 1*E*). Mice injected with the fluorescent isotype control showed the fluorescent fungal elements only without an isotype-derived second fluorescent signal (Fig. 1*E*). These experiments show that JF5 specifically binds to the target mannoprotein antigen in *A. fumigatus*-infected lungs in vivo and therefore qualifies as a potential diagnostic agent for whole-body molecular imaging using PET/MRI.

**[$^{64}$Cu]DOTA-JF5 Specifically Detects *A. fumigatus* Infection in Vivo.** For immunoPET imaging, JF5 was conjugated with the chelator DOTA and then labeled with the radionuclide $^{64}$Cu, which allows consecutive imaging for up to 3 d. Neutropenic mice infected with *A. fumigatus* were injected with [$^{64}$Cu]DOTA-JF5 and the distribution of the tracer was evaluated by PET following MRI at 3, 24, and 48 h after infection (Fig. 2 and Fig. S2). To evaluate the specificity of [$^{64}$Cu]DOTA-JF5, biodistribution studies with several control infection models were performed. Animals were i.t. infected with *A. fumigatus* or the bacterial pathogen *Streptococcus pneumoniae*, or systemically with the bacterial pathogen *Yersinia enterocolitica*, and the in vivo biodistribution of [$^{64}$Cu]DOTA-JF5 was assessed 3, 24, and 48 h later by PET/MRI (Fig. 2 and Fig. S2). PET images revealed a significantly elevated uptake of [$^{64}$Cu]DOTA-JF5 in the lungs of *A. fumigatus*-infected animals compared with lungs of PBS-treated control mice or mice infected with *S. pneumoniae* or *Y. enterocolitica* (Fig. 2*A*). The PET signal colocalized with the fungal lesions observed in the MR images. The mean [$^{64}$Cu]DOTA-JF5 uptake 48 h postinfection (hpi) in the lungs of the imaged mice was lowest in *Y. enterocolitica*-infected animals with 4.4 ± 0.3%ID/cc, followed by *S. pneumoniae*-infected and PBS-treated mice (5.2 ± 0.2; 5.9 ± 0.6%ID/cc). Compared with these controls, tracer uptake was significantly higher in the lungs of *A. fumigatus*-infected mice (11.9 ± 1.3%ID/cc) (Fig. 2*B*). The ex vivo biodistribution 48 hpi showed a significantly elevated uptake of [$^{64}$Cu]DOTA-JF5 with 34.6 ± 7.4%ID/g in *A. fumigatus*-infected lung tissue compared with the lungs of PBS controls (7.7 ± 2.0%ID/g), *S. pneumoniae* (8.1 ± 0.6%ID/g) and *Y. enterocolitica* (8.1 ± 1.5%ID/g) infected mice (Fig. 2*C*). A significant higher uptake of the tracer was already detectable 24 h after infection (Fig. S1). The discrepancy of approximately a factor of 2 in absolute quantification between %ID/g of post mortem biodistibution and in vivo small animal PET (%ID/cc) data are caused mainly by 511-keV photon attenuation in the animal and partial volume effects. However, the ratios of lungs and muscle tissue between the tested groups were similar in the in vivo PET quantification and the ex vivo gamma-counting (9). Besides increased signal intensity in the lung, we also found elevated signals in the blood, liver, spleen, and kidney. However, the analysis of fungal presence in these compartments using colony-forming unit (CFU) measurements revealed none to very limited colonization with the pathogen 48 h after infection (Fig. S3).

To further confirm the specificity of the [$^{64}$Cu]DOTA-JF5 tracer, blocking experiments were performed. Here, 1 mg of mannoprotein-specific IgM mAb ND12 or 1 mg of nonradiolabeled JF5 mAb were injected into infected animals 3 h before the injection of [$^{64}$Cu]DOTA-JF5 (Fig. 3*A*). In addition, the isotype control antibody MG3-35 was radiolabeled and injected in *A. fumigatus*-infected mice. The PET images showed the highest signal intensity in the lungs of *A. fumigatus*-infected nonblocked mice and decreased intensities in the relevant blocking controls (Fig. 3*A*), which was confirmed by ex vivo autoradiography of the lungs (Fig. 3*A*, *Lower*). The quantification of the data retrieved from the PET images 48 hpi (Fig. 3*B*) showed a reduced uptake from 10.2 ± 1.3%ID/cc

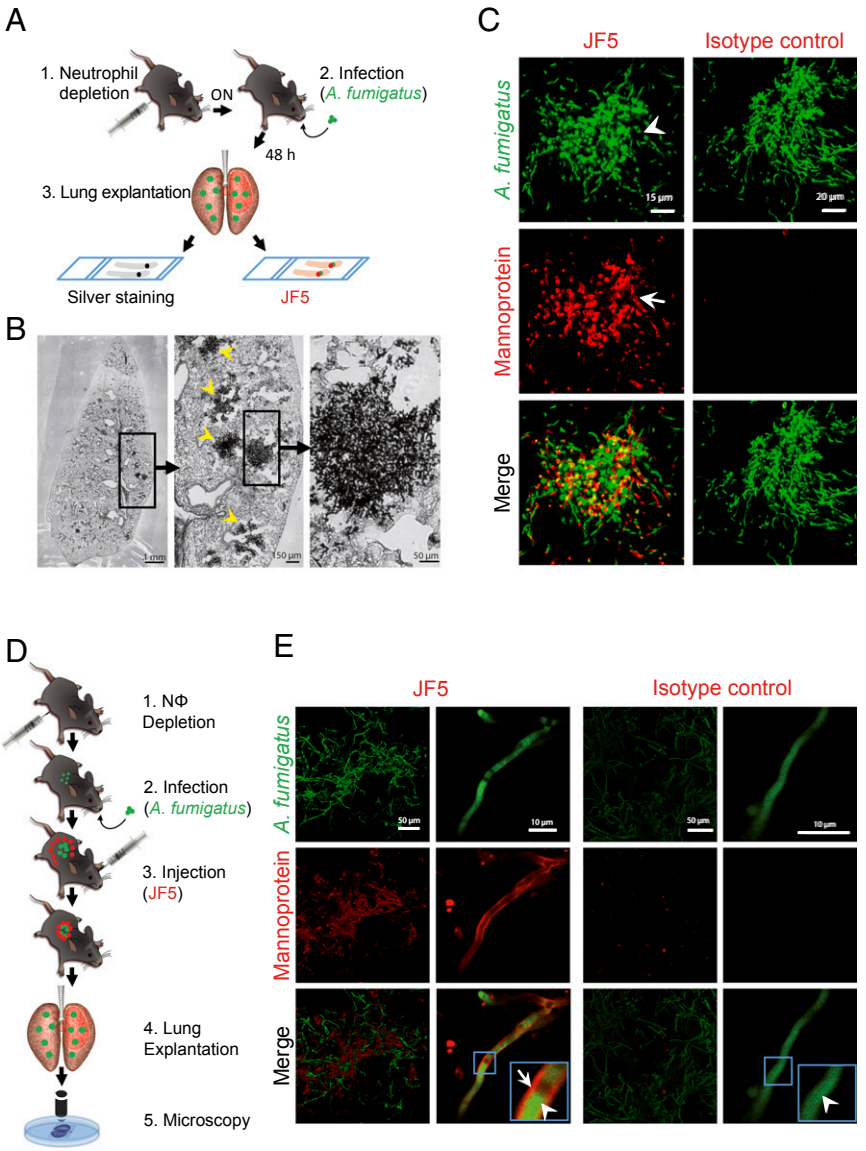


**Fig. 1.** Binding specificity of JF5 to *A. fumigatus* in infected mouse lungs. (*A*) Experimental workflow for the in situ binding of the mAb JF5: (1) Neutrophil depletion by i.p. injection of 100 μg anti-Gr-1 antibody (clone RB6-8C5) 17 h before infection. (2) Intratracheal infection with *A. fumigatus*$^{tdTomato}$. (3) After 48 h, lung explantation, fixation, and slicing followed by in situ staining with either JF5-DyLight650 or methenamine silver. (*B*) *A. fumigatus*-infected lung lobe section stained with methenamine silver. Fungal biomass can be detected by its black appearance (yellow arrowheads). (*C*) Tissue sections of *A. fumigatus*$^{tdTomato}$ (green) infected lungs stained with JF5-DyLight650 (displayed in false color red) or mouse IgG3 isotype control (red). White arrowheads indicate expression of tdTomato in the cytoplasm and JF5-antigen in the hyphal cell wall. (*D*) Experimental workflow for JF5 binding in vivo: (1) Neutrophil depletion by i.p. injection of 100 μg of anti-Gr-1 antibody (clone RB6-8C5) 17 h before infection. (2) Intratracheal infection with *A. fumigatus*$^{tdTomato}$. (3) i.v. injection of JF5-DyLight650 or fluorochrome-labeled mouse IgG3 isotype control 24 h after fungal infection. (4) Another 24 h later, lung explantation, followed by (5) in situ confocal microscopy of longitudinally sectioned lung. (*E*) Micrographs of *A. fumigatus*$^{tdTomato}$ (green) infected lungs treated with JF5-DyLight650 (red) or mouse IgG3 isotype control (red). Blue boxes indicate regions of interest, which are shown at higher magnification in the insets. White arrowheads indicate expression of tdTomato in the cytoplasm and white arrows indicate expression of JF5-antigen in the hyphal cell wall, respectively.

in the lungs of *A. fumigatus*-infected nonblocked animals down to 8.8 ± 2.2%ID/cc in the lungs of mice which received 1 mg of the blocking antibody JF5, 7.7 ± 2.0%ID/cc in the lungs of mice blocked with 1 mg ND12 and 8.0 ± 1.7%ID/cc in mice imaged with the radiolabeled isotype control mAb MG3-35. PBS-treated noninfected mice had significantly lower [$^{64}$Cu]DOTA-JF5 uptake in the lungs (6.0 ± 1.0%ID/cc) compared with the *A. fumigatus*-infected mice (Fig. 3*B*). Similar results were already evident at 24 hpi (Fig. S4).

Ex vivo biodistribution 48 hpi showed a significantly higher uptake of [$^{64}$Cu]DOTA-JF5 with 29.8 ± 7.4%ID/g in lung tissue of infected mice compared with PBS controls (9.0 ± 2.3%ID/g). A lower uptake was observed with the radiolabeled isotype control antibody MG3-35 (21.8 ± 0.7%ID/g). Also the blocking with 1mg ND12 (22.1 ± 3.3%ID/g) or JF5 (22.6 ± 8.1%ID/g) resulted in lower uptake of the tracer [$^{64}$Cu]DOTA-JF5 in infected lung tissue compared with the mice imaged solely with [$^{64}$Cu]DOTA-JF5 (positive control; Fig. 3*C*). Furthermore, the in vivo imaging results were confirmed by the ex vivo autoradiography where a high tracer uptake was seen in the lungs of the *A. fumigatus*-infected animals and a lower uptake was seen in the controls. The focal lesions of the fungus in the lungs of the *A. fumigatus*-infected animals perfectly matched with the accumulated radioactivity as revealed with the autoradiography.

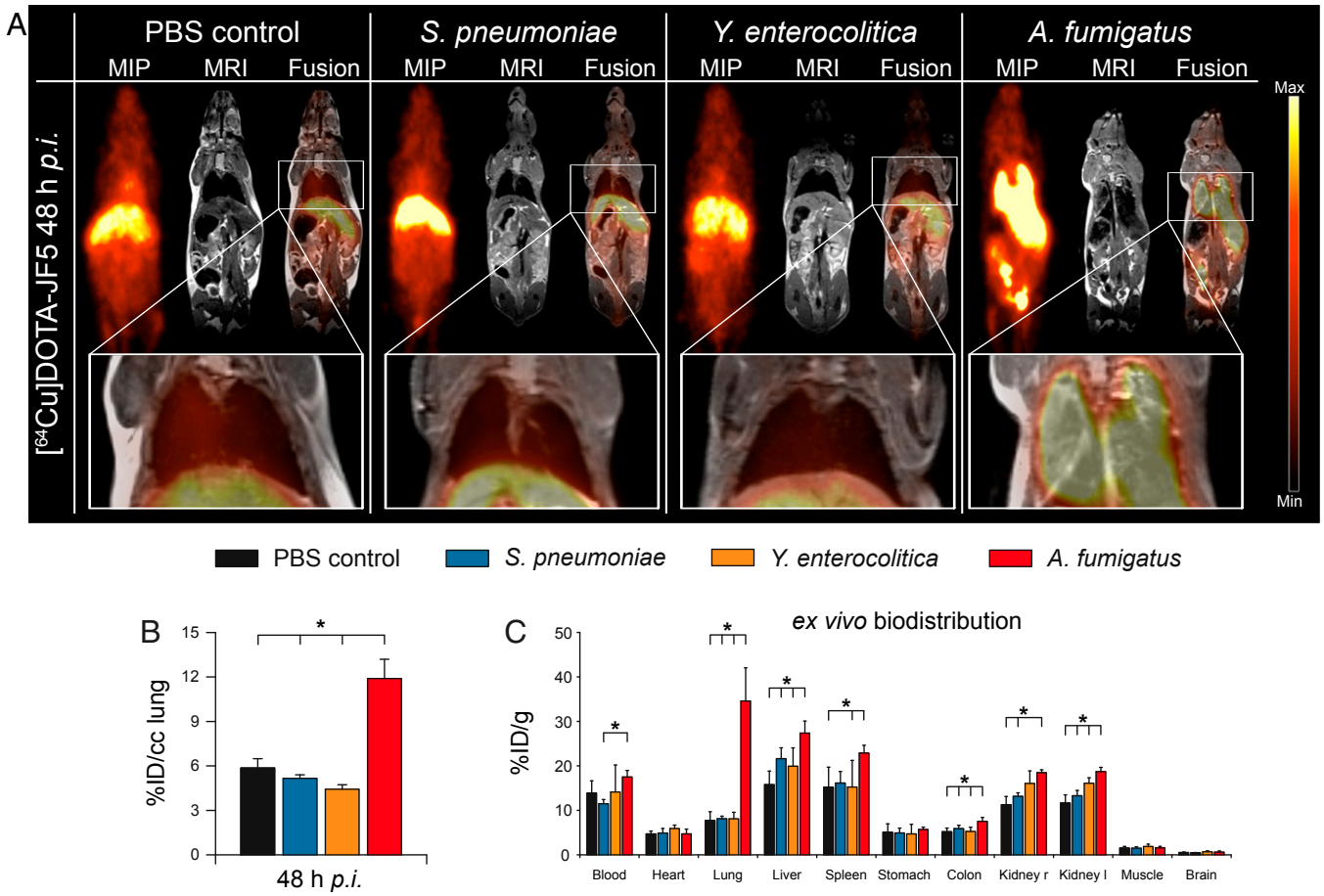


**Fig. 2.** [$^{64}$Cu]DOTA-JF5 as disease-specific PET-tracer for *A. fumigatus* lung infection. (*A*) Sagittal maximum intensity projections (MIP), MRI, and fused PET/MRI images of PBS-treated mice and *S. pneumoniae*-, *Y. enterocolitica*-, and *A. fumigatus*-infected mice injected with [$^{64}$Cu]DOTA-JF5 (48 h after infection). Tracer injection demonstrates highly specific accumulation in *A. fumigatus*-infected lung tissue compared with bacterial-infected or sham-treated animals. (*A*, *Lower*) Lungs of the respective animals. (*B*) Quantification of the in vivo PET images showed a significantly higher uptake of [$^{64}$Cu]DOTA-JF5 in the lungs of *A. fumigatus*-infected animals compared with the lungs of the control groups. (*C*) The ex vivo biodistribution confirmed the in vivo PET results with significantly higher uptake of [$^{64}$Cu]DOTA-JF5 in the lungs of *A. fumigatus*-infected animals compared with the lungs of control animals 48 hpi. The systemic infection at the late stage of the disease in neutropenic and *A. fumigatus*-infected animals is reflected by higher tracer accumulation in lymphatic and other organs. Black bars, PBS-treated controls ($n = 8$); blue bars, *S. pneumoniae*-infected mice ($n = 5$); orange bars, *Y. enterocolitica*-infected mice ($n = 5$); red bars, *A. fumigatus*-infected mice ($n = 5$). Data are expressed as the average ± SD (%ID/cc: PET; %ID/g: ex vivo biodistribution), one-way ANOVA, post hoc Tukey–Kramer corrected for multiple comparisons, $*P < 0.05$.

Examples of the autoradiography and the corresponding H&E staining are depicted in Fig. 3*A*, *Lower*.

**[$^{18}$F]FDG Does Not Allow Identification of *A. fumigatus* Infection.** The clinical standard for PET-based diagnosis in oncology is [$^{18}$F]FDG-PET. To study whether this tracer was able to discriminate between inflammatory processes and infections caused by fungal and bacterial pathogens, we performed [$^{18}$F]FDG-PET in animals infected with *A. fumigatus* and *S. pneumoniae*. [$^{18}$F]FDG-PET-imaging showed strong lung uptake of the tracer, irrespective of whether animals were infected with *A. fumigatus* or *S. pneumoniae*. Even animals that only received an i.t. administration of sterile PBS showed a clear uptake of [$^{18}$F]FDG 24 and 48 h after treatment (Fig. 4*A*). The %ID/cc in the lungs of *A. fumigatus*-infected animals between 3 and 48 h after infection rose from 4.7 ± 1.6 to 12.3 ± 1.8, whereas the %ID/cc in the lungs of the PBS-treated control animals increased from 3.1 ± 0.4 to 11.7 ± 3.1 (Fig. 4*B*). Likewise an increasing [$^{18}$F]FDG uptake was observed in the *S. pneumoniae* infected cohort with 3.4 ± 0.5%ID/cc (3 h) to 13.3 ± 4.6%ID/cc (48 h; Fig. 4*B*). The ex vivo biodistribution further confirmed the in vivo PET quantification, also showing no significant differences in the [$^{18}$F]FDG uptake of the various groups (Fig. 4*C*). These data demonstrated that the metabolism-sensitive tracer [$^{18}$F]FDG lacks specificity and thus is unable to distinguish between inflammation, sterile irritation and pathogen-induced infection and is incapable of identifying etiological agents of infection.

## Discussion

IPA is a leading cause of death in immunocompromised patients caused by the ubiquitous fungus *A. fumigatus* (2). The high rates of morbidity and mortality associated with this disease are due, to a large extent, to the paucity of diagnostic tests that allow accurate and rapid diagnosis followed by early treatment with mold-active drugs in patients presenting with fever of unknown origin (3). Currently, IPA is diagnosed based on clinical symptoms, radiology, and laboratory tests such as mycological culture, PCR, GM antigen tests, and microscopy (4, 10). However, most of these methods are unspecific and time consuming, impeding an early and accurate diagnosis. Radiology enables noninvasive identification of lung abnormalities, but technologies such as high-resolution CT, though able to visualize lung infections, are considered nonspecific and so are unable to discriminate between different fungal pathogens or to differentiate fungal

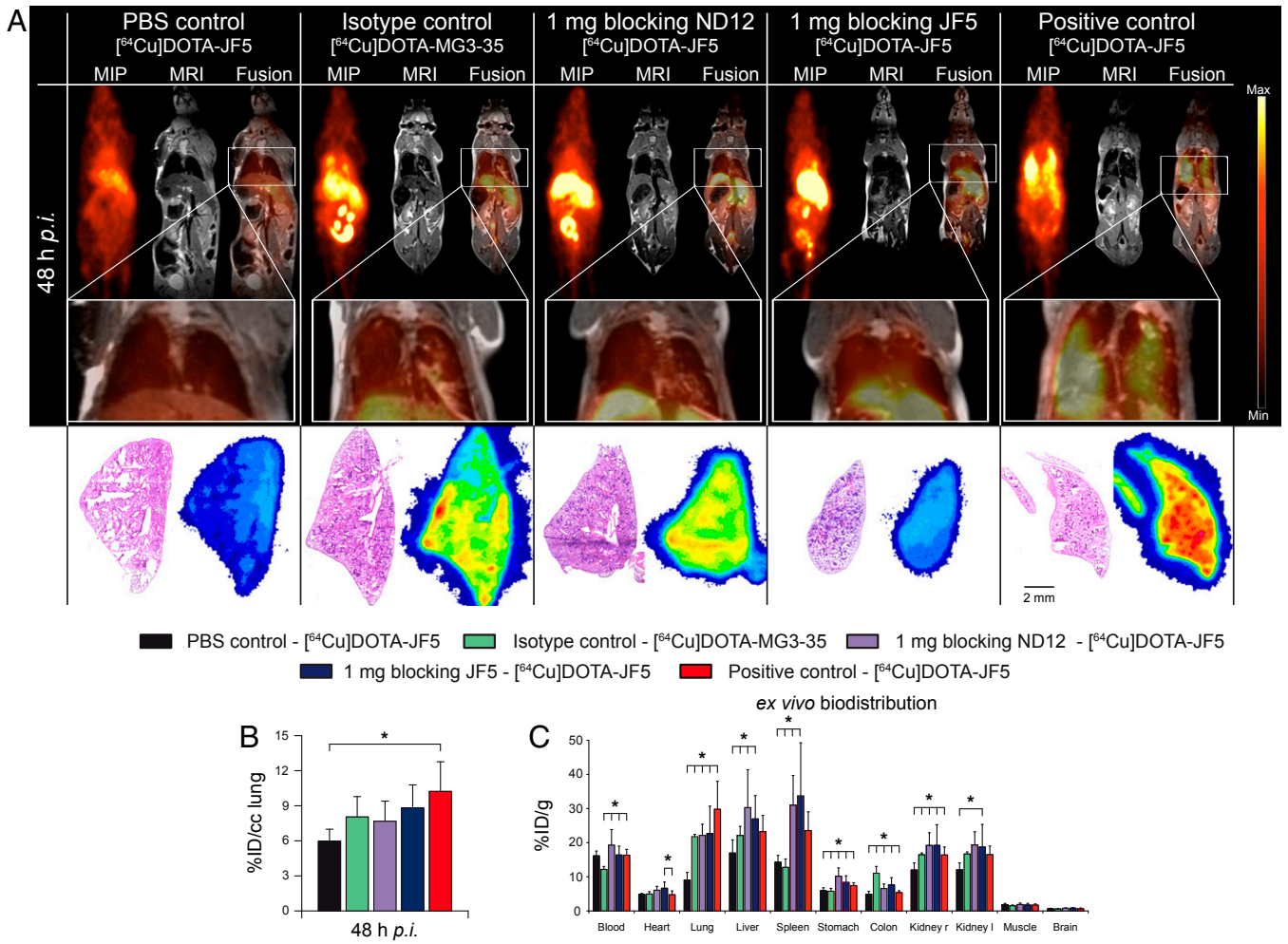


**Fig. 3.** JF5 binding is specific for *A. fumigatus*. (*A*) Sagittal MIP, MRI, and PET/MRI images of PBS-treated and *A. fumigatus*-infected mice. To test the specificity of the newly developed tracer, *A. fumigatus*-infected animals were either injected with a radiolabeled isotype control antibody (clone MG 3–35) or blocking experiments were performed. For blocking *A. fumigatus*-infected animals received 1 mg of nonradiolabeled ND12 or JF5 antibody 3 h prior the injection of the [$^{64}$Cu]DOTA-JF5. Tracer biodistribution demonstrates in PET images as high accumulation in *A. fumigatus*-infected lung tissue 48 hpi compared with PBS-treated, isotype control imaged or blocked lungs of the infected animals. (*A*, *Middle*) Lungs of the respective animals. (*A*, *Bottom*) The ex vivo autoradiography and the corresponding H&E staining of the slides show the strong accumulation of the tracer [$^{64}$Cu]DOTA-JF5 in the lungs of the infected animals in contrast to the controls. (*B*) Quantification of the in vivo PET images showed a higher uptake of [$^{64}$Cu]DOTA-JF5 in the lungs of *A. fumigatus*-infected animals compared with the lungs of the PBS controls, imaging with the radiolabeled MG 3–35 (isotype control) and the blocking experiments. (*C*) The ex vivo biodistribution confirmed the in vivo PET results with significantly higher uptake of [$^{64}$Cu]DOTA-JF5 in the lungs of *A. fumigatus*-infected animals compared with the lungs of PBS control animals. Black bars, PBS-treated controls; green bars, *A. fumigatus*-infected mice imaged with the radiolabeled isotype control antibody MG3-35 ($n = 5$); purple bars, *A. fumigatus*-infected mice blocked with 1 mg of IgM ND12 antibody ($n = 5$), blue bars, *A. fumigatus*-infected mice blocked with 1 mg of nonradiolabeled JF5 antibody ($n = 10$); red bars, *A. fumigatus*-infected mice ($n = 9$). Data are expressed as the average ± SD (%ID/cc: PET; %ID/g: ex vivo biodistribution), one-way ANOVA, post hoc Tukey–Kramer corrected for multiple comparisons, $^*P < 0.05$.

infections from other infectious etiologies. PET/MRI has proven to be a very powerful tool for diagnosis of cancer (11), but its use in infection diagnosis has so far been limited (6).

Existing tracers for PET imaging are not able to distinguish between malignancies and sterile or pathogen-induced inflammations (12, 13). Furthermore, it is even more challenging to correctly diagnose the cause of infection because the symptoms can manifest as nonpathogen-induced diseases such as malignancies (14–16). Although it has been reported that [$^{18}$F]FDG might serve as a useful imaging tool for initial diagnosis and therapy monitoring of IPA (16), our investigations have shown that increased [$^{18}$F]FDG uptake in *A. fumigatus*-infected lungs is indistinguishable from the uptake seen during inflammatory reactions due to sterile triggers or other pathogens. Recently, *A. fumigatus* detection based on single-photon emission tomography with $^{99m}$Tc-labeled morpholino-oligonucleotides specific for fungal 28S rRNA has been investigated (17). Although *A. fumigatus* lung infections are clearly discerned by using this technique, further investigations in other infectious models are needed to confirm the specificity of the probe.

PET-based imaging has seen enormous success in oncology (18–21), but has yet to be fully exploited for infection imaging (22, 23). Especially in the field of preclinical imaging, an increasing number of biologicals including small molecules, antibodies, their fragments and peptides have been developed and evaluated for imaging infectious diseases (24–28). Recently, attempts have been made to visualize IPA in *A. fumigatus*-infected animals with microPET/CT using $^{68}$Ga radiolabeled siderophores (29, 30). These small high-affinity chelating compounds are produced by fungi and bacteria to scavenge iron from the host, and by Gram-negative bacterial pathogens as virulence factors (31). Although rapid uptake of $^{68}$Ga by the *A. fumigatus* siderophore

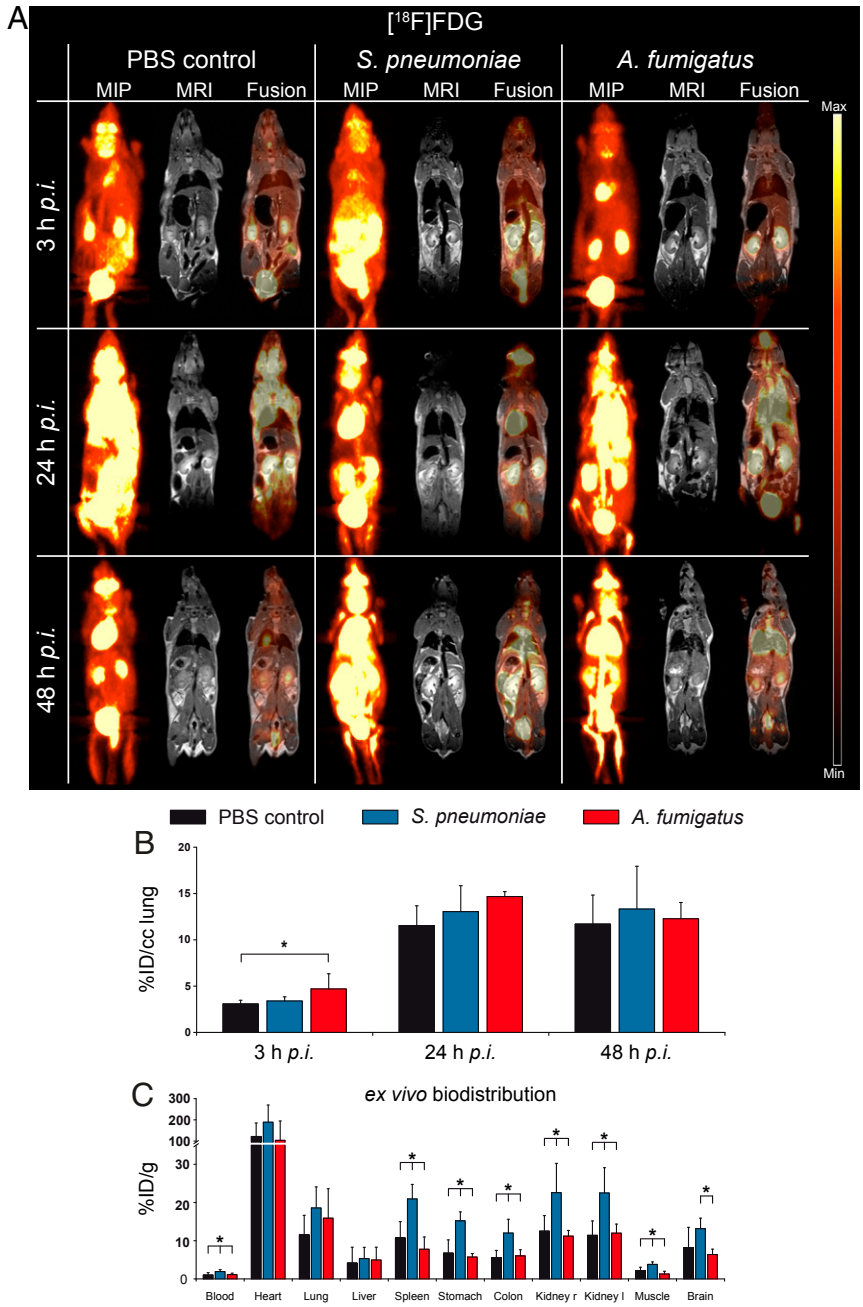


**Fig. 4.** [18F]FDG does not allow identification of *A. fumigatus* infection. (*A*) Sagittal MIP, MRI, and PET/MRI images of PBS-treated-, *S. pneumoniae*-, and *A. fumigatus*-infected mice imaged with [18F]FDG (3, 24, and 48 h after infection). All animals, including the PBS-treated mice, presented a highly elevated uptake of [18F]FDG within the lungs 24 and 48 h after the infection with *A. fumigatus* or *S. pneumoniae*. (*B*) Quantification of the in vivo PET images showed no significant differences in the uptake of [18F]FDG in the lungs of *A. fumigatus*-infected animals compared with the lungs of the control groups 24 and 48 h after infection. (*C*) The ex vivo biodistribution confirmed the in vivo [18F]FDG-PET results with no significant differences in the uptake of the lungs of *A. fumigatus*-infected animals compared with the lungs of control animals 48 hpi. Black bars, PBS-treated controls ($n = 10$); blue bars, *S. pneumoniae*-infected mice ($n = 5$); red bars, *A. fumigatus*-infected mice ($n = 5$). Data are expressed as the average ± SD (%ID/cc: PET; %ID/g: ex vivo biodistribution), one-way ANOVA, post hoc Tukey–Kramer corrected for multiple comparisons, $^*P < 0.05$.

TAFC has been shown to occur under conditions of iron depletion, patients who acquire fungal infections typically suffer from iron overload thereby potentially reducing tracer uptake and sensitivity of this method. Furthermore, TAFC-mediated $^{68}$Ga uptake has also been demonstrated in *Fusarium solani* and *Rhizopus oryzae*, invasive fungal pathogens that, like *Aspergillus*, cause disseminated infections in immunocompromised patients known as fusariosis and mucormycosis, respectively (32).

ImmunoPET has recently been used for tracking simian immunodeficiency virus (SIV) infection in macaques (33), and our work is, to our knowledge, the first example of its exploitation in the rapid and specific detection of a lethal fungal infection. Due to the long in vivo half-life of [$^{64}$Cu]DOTA-JF5 demonstrated here, we have shown that this immunoPET tracer would be an ideal candidate for repeated imaging of patients following a single injection of the radioactive tracer. Significantly, the JF5

antibody binds to a mannoprotein antigen released during active growth of the fungus only (34), and so is able to discriminate between infective hyphae and inactive spores, an important consideration given the abundance of *Aspergillus* spores in inhaled air. The hyphal-specific nature of our immunoPET tracer may therefore prove useful in monitoring infection in response to antifungal treatment. In the biodistribution analyses of infected animals, we found increased radioactive signals also in organs other than the infected lung. Signal enrichment in the liver might be due to nonspecific hepatic clearance of the radiolabeled antibody as seen by others (35), whereas nonspecific enrichment of radiolabeled antibody in kidney, blood, and spleen tissues has been reported in other immunoPET studies (33). Furthermore, in animals with IPA, it is likely that extracellular JF5 mannoprotein antigen released from infectious foci in the lungs accumulates in organs following shedding and circulation in the bloodstream, because the antigen is readily detectable in the serum of neutropenic animals and humans suffering from IPA (34, 36, 37). The methodology is essentially translatable to humans because the JF5 antibody detects a signature molecule of *A. fumigatus* infection that is clinically validated for IPA diagnosis in neutropenic patients using bronchoalveolar lavage fluids and point-of-care diagnostics (38). To this end, the antibody has been fully humanized to enable its use in human disease detection. A humanized version of the tracer would allow noninvasive identification of IPA in immunocompromised patients and monitoring of responsiveness to antifungal treatment.

## Materials and Methods

Additional and detailed information are provided in *SI Materials and Methods*.

All animal experiments were performed according to the German Animal Protection Law with permission from the Regierungspräsidium Tübingen and Magdeburg, Landesamt für Natur, Umwelt und Verbraucherschutz Nordrhein-Westfalen, and the Niedersächsische Landesamt für Verbraucherschutz und Lebensmittelsicherheit Braunschweig/Oldenburg, Germany. Neutropenic C57BL/6 OlaHsd mice were i.t. infected with a freshly prepared *A. fumigatus* spore suspension ($4 \times 10^6$ per mL). Animals of the control groups were i.t. infected with $1 \times 10^6$ CFUs of *S. pneumoniae* bacteria, i.v. injected with $5 \times 10^4$ CFUs of *Y. enterocolitica* bacteria or i.t. inoculated with 100 μL of PBS, respectively. Successful infection was confirmed by CFU assays, where the bacterial and fungal load of various organs was assessed 24 and 48 h after the respective infection.

[$^{18}$F]FDG (10–11 MBq) was i.v injected into *A. fumigatus*- or *S. pneumoniae*-infected animals, and the respective control animals and PET and MR images were acquired 3, 24, and 48 h after the initial infection by using a small animal PET scanner (Inveon, Siemens Preclinical Solutions) and a 7 T small animal MR tomograph (Clinscan, Bruker Biospin MRI). PET images were normalized to each other, subsequently fused to the respective MR images, and analyzed by using Inveon Research Workplace software (Siemens Preclinical Solutions).

To generate the *A. fumigatus*-specific PET tracer [$^{64}$Cu]DOTA-JF5, the JF5-secreting *A. fumigatus*-specific IgG3 mAb hybridoma cell line, which was characterized previously (34), was used. JF5 was purified with a HiTrap Protein G HP column (GE Healthcare Life Sciences), chelator conjugated with 10 mg/mL DOTA-NHS (Chematech), and subsequently radiolabeled with $^{64}$Cu which was created by proton irradiation of enriched $^{64}$Ni metal (35-75 mg; Isoflex, >95% enrichment) electroplated on a silver disk via the $^{64}$Ni(p,n)$^{64}$Cu nuclear reaction (39). *A. fumigatus*-, *S. pneumoniae*-, or *Y. enterocolitica*-infected animals and the respective control mice were consecutively imaged in PET and MRI 3, 24, and 48 h after the infection and i.v. injection of [$^{64}$Cu]DOTA-JF5. To assess the specificity of the newly developed PET tracer, blocking studies were performed. 1 mg of purified *Aspergillus* mannoprotein-specific IgM mAb ND12 or 1 mg of purified nonradiolabeled JF5 antibody were i.v. injected into *A. fumigatus*-infected animals 3 h before the injection of the radiolabeled JF5. Static 10-min PET scans were performed 3, 24, and 48 h after application of the tracer. Additionally, an unspecific IgG3 isotype control antibody (MG3-35, Biolegend) was radiolabeled as described previously and i.v. injected into *A. fumigatus*-infected animals.

After the final PET scan, an ex vivo biodistribution of various organs was performed in the γ-counter (Wallac 1480 WIZARD 3″ Gamma Counter; Perkin-Elmer) and an ex vivo autoradiography with subsequent H&E staining of the tissue slices was accomplished.

For application in fluorescence microscopy, purified JF5 mAb was coupled to DyLight 650 (Thermo Fisher Scientific) and *A. fumigatus*-infected lung slices were in situ stained with the fluorescently labeled JF5 or with the fluorescently labeled IgG3 isotype control MG3-35. For in vivo staining, *A. fumigatus*-infected mice were i.v. injected with the fluorochrome-labeled JF5 or the unspecific isotype control and lungs were explanted 48 h after the infection for microscopy.

Statistical significance was determined by using a two-tailed *t* test. For experiments with more than two investigated groups, statistical significances were calculated by using one-way analysis of variance (ANOVA) followed by Tukey's Multiple Comparison Test conducted with Origin 8 software (OriginLab).

**ACKNOWLEDGMENTS.** We thank the Imaging Center Essen (IMCES) for help with optical imaging and Andreas Jeron (Otto-von-Guericke University of Magdeburg) for the generation of rendered 3D objects to illustrate the experimental workflow in Fig. 1 and Eileen Bergmüller for help with conjugating antibodies for histology. We thank Maren Harant, Sandro Aidone, and Ramona Stumm for excellent technical assistance. This work was supported by the European Union Seventh Framework Programme FP7/2007-2013 under Grant 602820 and by the Deutsche Forschungsgemeinschaft Grant WI 3777/1-2.

1. WHO (2014) World Health Statistics 2014. Available at apps.who.int/iris/bitstream/10665/112738/1/9789240692671_eng.pdf. Accessed August 10, 2015.
2. Brown GD, et al. (2012) Hidden killers: Human fungal infections. *Sci Transl Med* 4(165):165rv13.
3. Freifeld AG, et al.; Infectious Diseases Society of America (2011) Clinical practice guideline for the use of antimicrobial agents in neutropenic patients with cancer: 2010 update by the infectious diseases society of america. *Clin Infect Dis* 52(4):e56–e93.
4. Hope WW, Walsh TJ, Denning DW (2005) Laboratory diagnosis of invasive aspergillosis. *Lancet Infect Dis* 5(10):609–622.
5. Prattes J, et al. (2014) Novel tests for diagnosis of invasive aspergillosis in patients with underlying respiratory diseases. *Am J Respir Crit Care Med* 190(8):922–929.
6. Glaudemans AW, Quintero AM, Signore A (2012) PET/MRI in infectious and inflammatory diseases: Will it be a useful improvement? *Eur J Nucl Med Mol Imaging* 39(5):745–749.
7. Signore A, Mather SJ, Piaggio G, Malviya G, Dierckx RA (2010) Molecular imaging of inflammation/infection: Nuclear medicine and optical imaging agents and methods. *Chem Rev* 110(5):3112–3145.
8. Wehrl HF, et al. (2014) Preclinical and Translational PET/MR Imaging. *J Nucl Med* 55:(Supplement 2):11S–18S.
9. Elsässer-Beile U, et al. (2009) PET imaging of prostate cancer xenografts with a highly specific antibody against the prostate-specific membrane antigen. *J Nucl Med* 50(4):606–611.
10. Reichenberger F, Habicht JM, Gratwohl A, Tamm M (2002) Diagnosis and treatment of invasive pulmonary aspergillosis in neutropenic patients. *Eur Respir J* 19(4):743–755.
11. Pichler BJ, Kolb A, Nägele T, Schlemmer HP (2010) PET/MRI: Paving the way for the next generation of clinical multimodality imaging applications. *J Nucl Med* 51(3):333–336.
12. Coombes JL, Robey EA (2010) Dynamic imaging of host-pathogen interactions in vivo. *Nat Rev Immunol* 10(5):353–364.
13. Signore A, Glaudemans AW (2011) The molecular imaging approach to image infections and inflammation by nuclear medicine techniques. *Ann Nucl Med* 25(10):681–700.
14. Glaudemans AW, Signore A (2010) FDG-PET/CT in infections: The imaging method of choice? *Eur J Nucl Med Mol Imaging* 37(10):1986–1991.
15. Guimarães MD, et al. (2013) Fungal infection mimicking pulmonary malignancy: Clinical and radiological characteristics. *Lung* 191(6):655–662.
16. Hot A, et al. (2011) Diagnostic contribution of positron emission tomography with [18F]fluorodeoxyglucose for invasive fungal infections. *Clin Microbiol Infect* 17(3):409–417.
17. Wang Y, et al. (2013) Detection of Aspergillus fumigatus pulmonary fungal infections in mice with (99m)Tc-labeled MORF oligomers targeting ribosomal RNA. *Nucl Med Biol* 40(1):89–96.
18. Harry VN, Semple SI, Parkin DE, Gilbert FJ (2010) Use of new imaging techniques to predict tumour response to therapy. *Lancet Oncol* 11(1):92–102.
19. Mortimer JE, et al. (2014) Functional imaging of human epidermal growth factor receptor 2-positive metastatic breast cancer using (64)Cu-DOTA-trastuzumab PET. *J Nucl Med* 55(1):23–29.
20. Tamura K, et al. (2013) 64Cu-DOTA-trastuzumab PET imaging in patients with HER2-positive breast cancer. *J Nucl Med* 54(11):1869–1875.
21. Wu AM, Olafsen T (2008) Antibodies for molecular imaging of cancer. *Cancer J* 14(3):191–197.
22. Glaudemans AW, Slart RH, van Dijl JM, van Oosten M, van Dam GM (2015) Molecular imaging of infectious and inflammatory diseases: A terra incognita. *J Nucl Med* 56(5):659–661.
23. Signore A, Glaudemans AW, Galli F, Rouzet F (2015) Imaging infection and inflammation. *BioMed Res Int* 2015:615150.
24. Bunschoten A, Welling MM, Termaat MF, Sathekge M, van Leeuwen FW (2013) Development and prospects of dedicated tracers for the molecular imaging of bacterial infections. *Bioconjug Chem* 24(12):1971–1989.

25. Ning X, et al. (2014) PET imaging of bacterial infections with fluorine-18-labeled maltohexaose. *Angew Chem Int Ed Engl* 53(51):14096–14101.
26. Weinstein EA, et al. (2014) Imaging Enterobacteriaceae infection in vivo with 18F-fluorodeoxysorbitol positron emission tomography. *Sci Transl Med* 6(259):259ra146.
27. Langer O, et al. (2005) In vitro and in vivo evaluation of [18F]ciprofloxacin for the imaging of bacterial infections with PET. *Eur J Nucl Med Mol Imaging* 32(2):143–150.
28. Mills B, et al. (2015) [(18)F]FDG-6-P as a novel in vivo tool for imaging staphylococcal infections. *EJNMMI Res* 5:13.
29. Haas H, Petrik M, Decristoforo C (2015) An iron-mimicking, Trojan horse-entering fungi–has the time come for molecular imaging of fungal infections? *PLoS Pathog* 11(1):e1004568.
30. Petrik M, et al. (2010) 68Ga-siderophores for PET imaging of invasive pulmonary aspergillosis: Proof of principle. *J Nucl Med* 51(4):639–645.
31. Holden VI, Bachman MA (2015) Diverging roles of bacterial siderophores during infection. *Metallomics* 7(6):986–995.
32. Thornton CR, Wills OE (2015) Immunodetection of fungal and oomycete pathogens: Established and emerging threats to human health, animal welfare and global food security. *Crit Rev Microbiol* 41(1):27–51.
33. Santangelo PJ, et al. (2015) Whole-body immunoPET reveals active SIV dynamics in viremic and antiretroviral therapy-treated macaques. *Nat Methods* 12(5):427–432.
34. Thornton CR (2008) Development of an immunochromatographic lateral-flow device for rapid serodiagnosis of invasive aspergillosis. *Clin Vaccine Immunol* 15(7): 1095–1105.
35. Tavaré R, et al. (2014) Engineered antibody fragments for immuno-PET imaging of endogenous CD8+ T cells in vivo. *Proc Natl Acad Sci USA* 111(3):1108–1113.
36. White PL, Parr C, Thornton C, Barnes RA (2013) Evaluation of real-time PCR, galactomannan enzyme-linked immunosorbent assay (ELISA), and a novel lateral-flow device for diagnosis of invasive aspergillosis. *J Clin Microbiol* 51(5):1510–1516.
37. Wiederhold NP, et al. (2013) Interlaboratory and interstudy reproducibility of a novel lateral-flow device and influence of antifungal therapy on detection of invasive pulmonary aspergillosis. *J Clin Microbiol* 51(2):459–465.
38. Pan Z, et al. (2015) Diagnostic accuracy of a novel lateral-flow device in invasive aspergillosis: A meta-analysis. *J Med Microbiol* 64(7):702–707.
39. Wiehr S, et al. (2014) Pharmacokinetics and PET imaging properties of two recombinant anti-PSMA antibody fragments in comparison to their parental antibody. *Prostate* 74(7):743–755.
40. Hearn VM, Mackenzie DW (1980) Mycelial antigens from two strains of Aspergillus fumigatus: An analysis by two-dimensional immunoelectrophoresis. *Mykosen* 23(10): 549–562.
41. Hasenberg A, et al. (2015) Catchup: A mouse model for imaging-based tracking and modulation of neutrophil granulocytes. *Nat Methods* 12(5):445–452.
42. Hasenberg M, Köhler A, Bonifatius S, Jeron A, Gunzer M (2011) Direct observation of phagocytosis and NET-formation by neutrophils in infected lungs using 2-photon microscopy. *J Vis Exp* 52:2659.
43. Hamacher K, Coenen HH, Stöcklin G (1986) Efficient stereospecific synthesis of no-carrier-added 2-[18F]-fluoro-2-deoxy-D-glucose using aminopolyether supported nucleophilic substitution. *J Nucl Med* 27(2):235–238.